Stoch Environ Res Risk Assess
DOI 10.1007/s00477-007-0198-y

ORIGINAL PAPER

Stochastic analysis of transient three-phase flow in heterogeneous porous media

Mingjie Chen · Arturo A. Keller · Zhiming Lu

Abstract In this manuscript, we extend the stochastic analysis of transient two-phase flow (Chen et al., Water Resour Res 42:W03425, 2006) to three-phase flow, i.e., water, air, and NAPL. We use the van Genuchten model and the Parker and Lenhard three-phase model to describe the relationships between phase saturation, phase relative permeability, and capillary pressure. The log-transformations of intrinsic permeability $Y(\mathbf{x}) = \ln k(\mathbf{x})$, soil pore size distribution parameter $\beta_{ow}(\mathbf{x}) = \ln \alpha_{ow}(\mathbf{x})$ between water and NAPL, and $\beta_{ao}(\mathbf{x}) = \ln \alpha_{ao}(\mathbf{x})$ between air and NAPL, and van Genuchten fitting parameter $\bar{n}(\mathbf{x}) = \ln [n(\mathbf{x}) - 1]$, are treated as stochastic variables that are normally distributed with a separable exponential covariance model. The Karhunen–Loeve expansion and perturbation method (KLME) is used to solve the resulting equations. We evaluate the stochastic model using two-dimensional examples of three-phase flow with NAPL leakage. We also conduct Monte Carlo (MC) simulations to verify the stochastic model. A comparison of results from MC and KLME indicates the validity of the proposed KLME application in three-phase flow. The computational efficiency of the KLME approach over MC methods is at least an order of magnitude for three-phase flow problems. This verified stochastic model is then used to investigate the sensitivity of fluid saturation variances to the input variances.

M. Chen (✉) · Z. Lu
Hydrology & Geochemistry Group (EES-6),
Los Alamos National Laboratory, Los Alamos, NM, USA
e-mail: mchen@lanl.gov

A. A. Keller
Bren School of Environmental Sciences and Management,
University of California, Santa Barbara, CA, USA

1 Introduction

Contamination of vadose zone and groundwater caused by Non-Aqueous-Phase-Liquid (NAPL) spills threatens subsurface water resources. Remediation of NAPL-contaminated groundwater requires comprehension of flow and transport of NAPL within the natural subsurface formation. It is recognized that soil heterogeneity plays a critical role in the migration of NAPL, and it may make deterministic modeling of flow systems impossible due to the lack of required field data to adequately represent it. Therefore, many researchers have resorted to stochastic approaches, which provide a more applicable and efficient method for analyzing subsurface flow, compared to deterministic modeling. Stochastic analysis has been studied extensively to simulate flow and transport in both saturated and unsaturated porous media in the last two decades (e.g., Dagan 1989; Gelhar 1993; Zhang 2002), though very little research has been conducted on multiphase flow. Chang et al. (1995a, b) used a spectral/perturbation method to analyze water–oil flow under saturated and unsaturated conditions and to evaluate the moments of the capillary pressure. Abdin et al. (1995, 1996) further demonstrated the validity of these spectral/perturbation analyses via numerical simulations. Ghanem and Dham (1998) used the spectral stochastic finite element method to discretize the governing stochastic two-phase flow equations in the Euclidian physical dimensions, and the random property in elements is expressed by Karhunen–Loeve expansion. Combined with polynomial

expansions, the moments are solved numerically. A novel stochastic approach based on the Karhunen–Loeve expansion and perturbation method (KLME) has been implemented in saturated flow and unsaturated one-phase flow by Zhang and Lu (2004) and Yang et al.(2004). Chen et al. (2005, 2006) introduced KLME method to complex multiphase flow systems, and predicted mean and variance of fluid pressures, capillary pressure and saturations for the water–oil flow.

These previous stochastic studies of multiphase flow in heterogeneous porous media have been limited to water–oil two phase flow or at most assuming a static gas phase, while in remediation processes the gas phase behavior and the interaction between the water, oil and air play a critical role in some situations. For example, gas venting is a popular method for soil remediation and cleanup, if the NAPLs are volatile. The idea of gas venting is to pump air to pass through the contaminated zone, and extract the contaminant by a vaporization process. The contaminant gas phase is extracted and treated at the surface. In such a remediation scheme, a full three-phase model is a must. In the petroleum industry, a petroleum reservoir is typically three-phase flow system, and the movement of oil toward producing wells is strongly against capillarity and heterogeneities in the porous medium (Trangenstein and Bell 1989). The presence of the gas phase is indispensable in reservoir simulation, especially for some enhanced recovery methods such as miscible gas flooding. Therefore, understanding the stochastic and dynamic behavior of the three phases (water, NAPL and air) is imperative. The only study to date, by Abdin and Kaluarachchi (1997a, b), applied spectral/perturbation methods to stochastic analysis of three-phase flow to predict the variability of capillary pressures.

The objective of this study is to evaluate the effect of soil heterogeneity on the mean and variances of fluid and capillary pressures as well as on the phase saturations of all three phase, and to demonstrate the applicability of the KLME analysis to three-phase flow. Log intrinsic permeability, log pore size distributions, and log van Genuchten fitting parameter are treated as input stochastic properties, distributed normally with a separable exponential covariance function. The Karhunen–Loeve expansions of these stochastic input variables was presented in Chen et al. (2005, 2006) for two-phase flow, and the application to three-phase flow follows that expansion. Monte Carlo (MC) simulations are conducted to confirm the validity of the KLME analysis and its numerical implementation. We also present one base case study and a series of cases, to investigate the sensitivity of fluid saturation variances to input variability, and to obtain insights into the effect of soil heterogeneity on three-phase flow.

2 Derivation of KLME for transient three-phase flow

The KLME method includes decomposing the independent random process (e.g., log transformed intrinsic permeability) using the Karhunen–Loeve expansion and expanding the dependent stochastic process (e.g., fluid pressure) using polynomial expansion and perturbation methods. With these expansions, we formulate a series of deterministic partial differential equations in different orders, which are called KL-based Moment Equations (KLME). These partial differential equations can be solved using existing numerical techniques and the solutions are assembled to construct mean and (co)variances of fluid pressures. In this section, we will derive KLME for transient water–oil–air flow in heterogeneous porous media.

Similarly to the fully coupled water–oil phase transient flow formulations (Chen et al. 2006), the basis three-phase flow equations are the phase conservation laws and the generalized Darcy law:

$$\phi \frac{\partial S_p(\mathbf{x},t)}{\partial t} + \nabla \cdot \mathbf{q}_p(\mathbf{x},t) = F_p(\mathbf{x},t), \tag{1}$$

$$\mathbf{q}_p(\mathbf{x},t) = -\lambda_p(\mathbf{x},t)\left[\nabla \cdot P_p(\mathbf{x},t) + \rho_p \mathbf{g}\right], \tag{2}$$

subject to initial and boundary conditions

$$P_p(\mathbf{x},0) = P_{p0}(\mathbf{x}), \quad \mathbf{x} \in \Omega, \tag{3}$$

$$P_p(\mathbf{x},t) = P_{pt}(\mathbf{x},t), \quad \mathbf{x} \in \Gamma_D, \tag{4}$$

$$\mathbf{q}_p(\mathbf{x},t) \cdot \mathbf{n}(\mathbf{x}) = Q_p(\mathbf{x},t), \quad \mathbf{x} \in \Gamma_N, \tag{5}$$

where p denotes three phases ($p = w, a, o$); $S_p(\mathbf{x},t)$ are the water (w), air (a), and oil (o) saturations; $\mathbf{q}_p(\mathbf{x},t)$ are the water, air and oil fluxes; $\mathbf{x}$ is the position vector in 2- or 3-D; $F_p(\mathbf{x},t)$ is a source or sink term; $\lambda_p(\mathbf{x},t) = k(\mathbf{x})k_{rp}(S_p)/\mu_p$ is liquid mobility; $P_p(\mathbf{x},t)$ is the fluid pressure; ρ_p is fluid density; k(x) is the intrinsic permeability of porous media; k_{rp} is the phase relative permeability; μ_p is the liquid dynamic viscosity; $P_{p0}(\mathbf{x})$ is the initial pressure in the domain Ω; $P_{pt}(\mathbf{x},t)$ is the prescribed pressure on a Dirichlet boundary segment Γ_D; $Q_p(\mathbf{x},t)$ is the prescribed fluid flux across Neumann boundary segments Γ_N; $\mathbf{g}$ is the gravity vector; n(x) is the outward unit vector normal to the boundary Γ_N, and ϕ is the porosity of the media.

Letting $Z_p(\mathbf{x},t) = \ln \lambda_p(\mathbf{x},t)$, and combining (1) and (2) gives the governing flow equation:

$$\begin{aligned} &\frac{\partial^2 P_p(\mathbf{x},t)}{\partial x_i^2} + \frac{\partial Z_p(\mathbf{x},t)}{\partial x_i}\left[\frac{\partial P_p(\mathbf{x},t)}{\partial x_i} + \rho_p g \delta_{i1}\right] \\ &= \exp\left[-Z_p(\mathbf{x},t)\right]\left[\phi \frac{\partial S_p(\mathbf{x},t)}{\partial t} - F_p(\mathbf{x},t)\right], \end{aligned} \tag{6}$$

subject to boundary conditions

$$P_p(\mathbf{x},0) = P_{p0}(\mathbf{x}), \quad \mathbf{x} \in \Omega, \tag{7}$$

$$P_p(\mathbf{x},t) = P_{pt}(\mathbf{x},t), \quad \mathbf{x} \in \Gamma_D, \tag{8}$$

$$n_i(\mathbf{x}) \exp\left[Z_p(\mathbf{x},t)\right]\left[\frac{\partial P_p(\mathbf{x},t)}{\partial x_i} + \rho_p g \delta_{i1}\right] = -Q_p(\mathbf{x},t), \quad \mathbf{x} \in \Gamma_N, \tag{9}$$

where, δ_{i1} is the Krönecker delta function, which equals 1 when i is 1 (upward direction) or 0 otherwise. The initial and boundary terms $P_{p0}(\mathbf{x})$ and $P_{pt}(\mathbf{x},t)$, the source–sink term $D_p(\mathbf{x},t)$, ϕ and S_{wr} are assumed to be deterministic.

In this study, the most widely used three-phase capillary pressure–saturation relationships derived from van Genuchten (1980) are used:

$$\overline{S}_w = \left[1 + (\alpha_{ow} P_{ow})^n\right]^{-m}, \tag{10}$$

$$\overline{S}_t = \left[1 + (\alpha_{ao} P_{ao})^n\right]^{-m}, \tag{11}$$

where $\overline{S}_w = (S_w - S_{wr})/(1 - S_{wr}), \overline{S}_t = (S_t - S_{wr})/(1 - S_{wr})$ are the effective water and effective total liquid saturation, $S_t = S_w + S_o$ is total liquid saturation, S_{wr} is residual water saturation, and $S_a = 1 - S_t$ is the air phase saturation. $P_{ow} = P_o - P_w$ and $P_{ao} = P_a - P_o$ are the water–oil and oil–air capillary pressures. Following the nomenclature of the Van Genuchten model, α_{ow}, α_{ao} are the oil–water and air–oil pore size distributions respectively, and n and m are fitting parameters with $m = 1 - 1/n$.

For relative permeability–saturation relationships, we employ Parker and Lenhard's model to the stochastic analysis of the transient water–oil two-phase flow. The functions can be expressed as:

$$k_{rw} = \bar{S}_w^{1/2}\left[1 - \left(1 - \bar{S}_w^{1/m}\right)^m\right]^2, \tag{12}$$

$$k_{ra} = (1 - \bar{S}_t)^{1/2}\left(1 - \bar{S}_t^{1/m}\right)^{2m}, \tag{13}$$

$$k_{ro} = (\bar{S}_t - \bar{S}_w)^{1/2}\left[\left(1 - \bar{S}_w^{1/m}\right)^m - \left(1 - \bar{S}_t^{1/m}\right)^m\right]^2. \tag{14}$$

The log-transformed soil permeability $Y(\mathbf{x}) = \ln k(\mathbf{x})$, log-transformed water–oil and oil–air pore size distributions $\beta_{ow}(\mathbf{x}) = \ln \alpha_{ow}(\mathbf{x})$ and $\beta_{ao}(\mathbf{x}) = \ln \alpha_{ao}(\mathbf{x})$, and log-transformed van Genuchten parameter $\bar{n}(\mathbf{x}) = \ln[n(\mathbf{x}) - 1]$ are treated as random space functions, by which $n(\mathbf{x})$ is guaranteed to be greater than 1. Although the KLME method does not require specification of probability distribution for random fields, we assume them to follow normal distribution for the sake of conducting MC simulations. These random variables are presented in phase mobility and the relationships between capillary pressures and saturations. Using these definitions, the governing equations (6)–(9) become stochastic partial differential equations, and the corresponding solutions are statistical moments of the dependent variables.

We use the same KLME approach presented in Chen et al. (2005, 2006) to approximate the solutions of these stochastic partial differential equations in terms of moments of pressure head. Based on Eqs. (40), (41) and (42) in Appendix A, the governing equation (6) can be extended as

$$\frac{\partial^2 P_w}{\partial x_i^2} + \frac{\partial Z_w}{\partial x_i}\left(\frac{\partial P_w}{\partial x_i} + \rho_w g \delta_{i1}\right) = \frac{C_{ow}}{e^{(Z_w)}}\frac{\partial P_{ow}}{\partial t} - \frac{F_w}{e^{(Z_w)}}, \tag{15}$$

$$\frac{\partial^2 P_a}{\partial x_i^2} + \frac{\partial Z_a}{\partial x_i}\left(\frac{\partial P_a}{\partial x_i} + \rho_a g \delta_{i1}\right) = \frac{C_{ao}}{e^{(Z_a)}}\frac{\partial P_{ao}}{\partial t} - \frac{F_a}{e^{(Z_a)}}, \tag{16}$$

$$\frac{\partial^2 P_o}{\partial x_i^2} + \frac{\partial Z_o}{\partial x_i}\left(\frac{\partial P_o}{\partial x_i} + \rho_o g \delta_{i1}\right) = \frac{-C_{ow}}{e^{(Z_o)}}\frac{\partial P_{ow}}{\partial t} + \frac{-C_{ao}}{e^{(Z_o)}}\frac{\partial P_{ao}}{\partial t} - \frac{F_o}{e^{(Z_o)}}. \tag{17}$$

To simplify the expression, we removed $(\mathbf{x},t)$ from the location and time dependent variables in the above equations, as well as in the following equations. The boundary conditions are the same as those shown in (7)–(9). $Z_p(\mathbf{x},t)$, $C_{ow}(\mathbf{x},t)$, and $C_{ao}(\mathbf{x},t)$ are derived in Appendix A. One may expand them into infinite series: $P_p(\mathbf{x},t) = P_p^{(0)} + P_p^{(1)} + \cdots, Z_p(\mathbf{x},t) = Z_p^{(0)} + Z_p^{(1)} + \cdots$, $P_{ow}(\mathbf{x},t) = P_{ow}^{(0)} + P_{ow}^{(1)} + \cdots$, $P_{ao}(\mathbf{x},t) = P_{ao}^{(0)} + P_{ao}^{(1)} + \cdots, C_{ow}(\mathbf{x},t) = C_{ow}^{(0)} + C_{ow}^{(1)} + \cdots$, and $C_{ao}(\mathbf{x},t) = C_{ao}^{(0)} + C_{ao}^{(1)} + \cdots$. In these series, the order of each term is with respect to σ_s, which is some combination of the variability of the input variables. Substituting these decompositions into (15)–(17), and collecting like terms at the same order leads to the partial differential equations for 0th and 1st order as follows:

$$\frac{\partial^2 P_w^{(0)}}{\partial x_i^2} + \frac{\partial Z_w^{(0)}}{\partial x_i}\left[\frac{\partial P_w^{(0)}}{\partial x_i} + \rho_w g \delta_{i1}\right] = \frac{C_{ow}^{(0)}}{e^{\left[Z_w^{(0)}\right]}}\frac{\partial P_{ow}^{(0)}}{\partial t} - \frac{F_w}{e^{\left[Z_w^{(0)}\right]}}, \tag{18}$$

$$\frac{\partial^2 P_a^{(0)}}{\partial x_i^2} + \frac{\partial Z_a^{(0)}}{\partial x_i}\left[\frac{\partial P_a^{(0)}}{\partial x_i} + \rho_a g \delta_{i1}\right] = \frac{C_{ao}^{(0)}}{e^{\left[Z_a^{(0)}\right]}}\frac{\partial P_{ao}^{(0)}}{\partial t} - \frac{F_a}{e^{\left[Z_a^{(0)}\right]}}, \tag{19}$$

$$\frac{\partial^2 P_o^{(0)}}{\partial x_i^2} + \frac{\partial Z_o^{(0)}}{\partial x_i}\left[\frac{\partial P_o^{(0)}}{\partial x_i} + \rho_o g \delta_{i1}\right] = \frac{-C_{ow}^{(0)}}{e^{\left[Z_o^{(0)}\right]}}\frac{\partial P_{ow}^{(0)}}{\partial t} + \frac{-C_{ao}^{(0)}}{e^{\left[Z_o^{(0)}\right]}}\frac{\partial P_{ao}^{(0)}}{\partial t} - \frac{F_o}{e^{\left[Z_o^{(0)}\right]}}, \tag{20}$$

$$P_p^{(0)}(\mathbf{x},0) = P_{p0}(\mathbf{x}), \quad \mathbf{x} \in \Omega, \tag{21}$$

$$P_p^{(0)}(\mathbf{x},t) = P_{pt}(\mathbf{x},t), \quad \mathbf{x} \in \Gamma_D, \tag{22}$$

$$n_i(\mathbf{x})\left[\frac{\partial P_p^{(0)}(\mathbf{x},t)}{\partial x_i}+\rho_p g\delta_{i1}\right]=\frac{-Q_p(\mathbf{x},t),}{\exp\left[Z_p^{(0)}(\mathbf{x},t)\right]},\quad \mathbf{x}\in\Gamma_N, \tag{23}$$

and

$$\frac{\partial^2 P_w^{(1)}}{\partial x_i^2}+J_{wi}\frac{\partial Z_w^{(1)}}{\partial x_i}+\frac{\partial Z_w^{(0)}}{\partial x_i}\frac{\partial P_w^{(1)}}{\partial x_i}=-\frac{F_w}{e^{Z_w^{(0)}}}Z_w^{(1)}+\frac{C_{ow}^{(0)}}{e^{Z_w^{(0)}}}\left[\frac{\partial P_{ow}^{(1)}}{\partial t}-Z_w^{(1)}\frac{\partial P_{ow}^{(0)}}{\partial t}\right]+\frac{C_{ow}^{(1)}}{e^{Z_w^{(0)}}}\frac{\partial P_{ow}^{(0)}}{\partial t}, \tag{24}$$

$$\frac{\partial^2 P_a^{(1)}}{\partial x_i^2}+J_{ai}\frac{\partial Z_a^{(1)}}{\partial x_i}+\frac{\partial Z_a^{(0)}}{\partial x_i}\frac{\partial P_a^{(1)}}{\partial x_i}=-\frac{F_a}{e^{Z_a^{(0)}}}Z_a^{(1)}+\frac{C_{ao}^{(0)}}{e^{Z_a^{(0)}}}\left[\frac{\partial P_{ao}^{(1)}}{\partial t}-Z_a^{(1)}\frac{\partial P_{ao}^{(0)}}{\partial t}\right]+\frac{C_{ao}^{(1)}}{e^{Z_a^{(0)}}}\frac{\partial P_{ao}^{(0)}}{\partial t}, \tag{25}$$

$$\frac{\partial^2 P_o^{(1)}}{\partial x_i^2}+J_{oi}\frac{\partial Z_o^{(1)}}{\partial x_i}+\frac{\partial Z_o^{(0)}}{\partial x_i}\frac{\partial P_o^{(1)}}{\partial x_i}=-\frac{F_o}{e^{Z_o^{(0)}}}Z_o^{(1)}-\frac{C_{ow}^{(0)}}{e^{Z_o^{(0)}}}\left[\frac{\partial P_{ow}^{(1)}}{\partial t}-Z_o^{(1)}\frac{\partial P_{ow}^{(0)}}{\partial t}\right]-\frac{C_{ow}^{(1)}}{e^{Z_o^{(0)}}}\frac{\partial P_{ow}^{(0)}}{\partial t}-\frac{C_{ao}^{(0)}}{e^{Z_o^{(0)}}}\left[\frac{\partial P_{ao}^{(1)}}{\partial t}-Z_o^{(1)}\frac{\partial P_{ao}^{(0)}}{\partial t}\right]-\frac{C_{ao}^{(1)}}{e^{Z_o^{(0)}}}\frac{\partial P_{ao}^{(0)}}{\partial t}, \tag{26}$$

$$P_p^{(1)}(\mathbf{x},0)=0,\quad \mathbf{x}\in\Omega, \tag{27}$$

$$P_p^{(1)}(\mathbf{x},t)=0,\quad \mathbf{x}\in\Gamma_D, \tag{28}$$

$$n_i(\mathbf{x})\left[\frac{\partial P_p^{(1)}(\mathbf{x},t)}{\partial x_i}+J_{pi}(\mathbf{x},t)Z_p^{(1)}(\mathbf{x},t)\right]=0,\quad \mathbf{x}\in\Gamma_N, \tag{29}$$

where $J_{pi}(\mathbf{x},t)=\partial P_p^{(0)}(\mathbf{x},t)/\partial x_i+\rho_p g\delta_{i1}(p=w,a,o)$ is the spatial mean gradient of total water, air and oil pressure. $Z_p^{(0)}(\mathbf{x},t), C_{ow}^{(0)}(\mathbf{x},t), C_{ao}^{(0)}(\mathbf{x},t)$, and $Z_p^{(1)}(\mathbf{x},t)$, $C_{ow}^{(1)}(\mathbf{x},t), C_{ao}^{(1)}(\mathbf{x},t)$ are derived in Appendix A.

Substituting (67)–(70) in Appendix A into (24)–(29) yields the infinite series of $\{\xi_n\}$ on both sides. The summation of both sides equal to each other:

$$\frac{\partial^2 P_{w,n}^{(1)}}{\partial x_i^2}+J_{wi}\frac{\partial Z_{w,n}^{(1)}}{\partial x_i}+\frac{\partial Z_w^{(0)}}{\partial x_i}\frac{\partial P_{w,n}^{(1)}}{\partial x_i}=-\frac{F_w}{e^{Z_w^{(0)}}}Z_{w,n}^{(1)}+\frac{C_{ow}^{(0)}}{e^{Z_w^{(0)}}}\left[\frac{\partial P_{ow,n}^{(1)}}{\partial t}-Z_{w,n}^{(1)}\frac{\partial P_{ow}^{(0)}}{\partial t}\right]+\frac{C_{ow,n}^{(1)}}{e^{Z_w^{(0)}}}\frac{\partial P_{ow}^{(0)}}{\partial t}, \tag{30}$$

$$\frac{\partial^2 P_{a,n}^{(1)}}{\partial x_i^2}+J_{ai}\frac{\partial Z_{a,n}^{(1)}}{\partial x_i}+\frac{\partial Z_a^{(0)}}{\partial x_i}\frac{\partial P_{a,n}^{(1)}}{\partial x_i}=-\frac{F_a}{e^{Z_a^{(0)}}}Z_{a,n}^{(1)}+\frac{C_{ao}^{(0)}}{e^{Z_a^{(0)}}}\left[\frac{\partial P_{ao,n}^{(1)}}{\partial t}-Z_{a,n}^{(1)}\frac{\partial P_{ao}^{(0)}}{\partial t}\right]+\frac{C_{ao,n}^{(1)}}{e^{Z_a^{(0)}}}\frac{\partial P_{ao}^{(0)}}{\partial t}, \tag{31}$$

$$\frac{\partial^2 P_{o,n}^{(1)}}{\partial x_i^2}+J_{oi}\frac{\partial Z_{o,n}^{(1)}}{\partial x_i}+\frac{\partial Z_o^{(0)}}{\partial x_i}\frac{\partial P_{o,n}^{(1)}}{\partial x_i}=-\frac{F_o}{e^{Z_o^{(0)}}}Z_{o,n}^{(1)}-\frac{C_{ow}^{(0)}}{e^{Z_o^{(0)}}}\left[\frac{\partial P_{ow,n}^{(1)}}{\partial t}-Z_{o,n}^{(1)}\frac{\partial P_{ow}^{(0)}}{\partial t}\right]-\frac{C_{ow,n}^{(1)}}{e^{Z_o^{(0)}}}\frac{\partial P_{ow}^{(0)}}{\partial t}-\frac{C_{ao}^{(0)}}{e^{Z_o^{(0)}}}\left[\frac{\partial P_{ao,n}^{(1)}}{\partial t}-Z_{o,n}^{(1)}\frac{\partial P_{ao}^{(0)}}{\partial t}\right]-\frac{C_{ao,n}^{(1)}}{e^{Z_o^{(0)}}}\frac{\partial P_{ao}^{(0)}}{\partial t}, \tag{32}$$

$$P_{p,n}^{(1)}(\mathbf{x},0)=0,\quad \mathbf{x}\in\Omega, \tag{33}$$

$$P_{p,n}^{(1)}(\mathbf{x},t)=0,\quad \mathbf{x}\in\Gamma_D, \tag{34}$$

$$n_i(\mathbf{x})\left[\frac{\partial P_{p,n}^{(1)}(\mathbf{x},t)}{\partial x_i}+J_{pi}(\mathbf{x},t)Z_{p,n}^{(1)}(\mathbf{x},t)\right]=0,\quad \mathbf{x}\in\Gamma_N, \tag{35}$$

where, $Z^{(1)}{}_{p,n}(\mathbf{x},t)$, and $C_{ow,n}^{(1)}(\mathbf{x},t), C_{ao,n}^{(1)}(\mathbf{x},t)$ are presented in Appendix A.

In this study, we approximate fluid pressure up to 1st order in σ_s:

$$P_p(\mathbf{x},t)\approx P_p^{(0)}(\mathbf{x},t)+P_p^{(1)}(\mathbf{x},t). \tag{36}$$

The mean fluid pressure is shown as

$$\left\langle P_p(\mathbf{x},t)\right\rangle\approx\left\langle P_p^{(0)}(\mathbf{x},t)\right\rangle+\left\langle P_p^{(1)}(\mathbf{x},t)\right\rangle=P_p^{(0)}(\mathbf{x},t). \tag{37}$$

Hence, the fluctuation of fluid pressure is

$$P_p'(\mathbf{x},t)\approx P_p(\mathbf{x},t)-\left\langle P_p(\mathbf{x},t)\right\rangle=P_p^{(1)}(\mathbf{x},t). \tag{38}$$

The covariance of fluid pressure can be derived as

$$C_{P_p}(\mathbf{x},\mathbf{y},t)=\sum_{n=1}^{\infty}P_{p,n}^{(1)}(\mathbf{x},t)P_{p,n}^{(1)}(\mathbf{y},t). \tag{39}$$

It is clear that covariance of fluid pressure $C_{P_p}(\mathbf{x},\mathbf{y},t)$ can be calculated from the solution of Eqs. (30)–(35), that is, $P^{(1)}{}_{p,n}(\mathbf{x},t)$. The covariance of fluid saturation can also be calculated based on the derivation in Appendix B. We use a finite difference scheme to discretize these coupled nonlinear partial differential equations and program the related code to the stochastic three-phase numerical model named "STO-3PHASE". It should be noted that all the equations and derivations presented above are formal, since one cannot be certain that all equations have a unique solution

in an appropriate functional space and are smooth enough to justify all the differentiations made.

3 Case 1: Comparison with Monte Carlo simulations

To test the simulator and the concepts and to demonstrate its validity, we conduct traditional MC simulations as the reference. To perform numerical simulations, the two-dimensional domain constructed by Chen et al. (2005, 2006) was considered in this work (Fig. 1). The 3 m × 0.96 m domain was discretized into 50 × 16 squares, each 0.06 m long. The soil properties, boundary conditions, and stochastic variables are given as Case 1 in Table 1. The output includes mean and variance of phase pressures (water, oil, air), capillary pressures (water–oil and air–oil), fluid saturations (water, oil, air). A constant oil leak is introduced at X1 = 2.4 m, X2 = 0.48 m, and constant water infiltration is specified at the top. At present the model requires constant boundary conditions. We considered a 100 kg/day of oil leak rate and water infiltrating at 0.5 cm/year, simulating a large spill into the domain, similar to an underground oil pipeline rupture. The Coefficient of Variation (CV) of intrinsic permeability, water–oil pore size distribution, oil–-air pore size distribution, and van Genuchten fitting parameters were 53.29, 10.08, 10.10, and 7.86% respectively. The number of MC simulations required depends on the variability of input variables. In the test cases, the variability was chosen to be relative small so that the flow simulation for each MC realization converges. Convergence was tested by plotting the mean and/or variance of the dependent variables at some selected locations for 2,000 simulations and evaluating whether they were stable. Statistical moments from 2,000 MC simulations were used to check the validity of the KLME simulations.

A comparison of the central vertical profile (X1) of the mean of the two capillary pressures shows a very good match between MC and KLME simulations after 1,000 days (Fig. 2a). Both oil–water capillary pressure P_{ow} and air–oil capillary pressure P_{ao} increase with elevation from a fixed boundary value at the bottom, with a deviation from linear behavior at the oil leak location. In this case, the magnitude of P_{ow} is larger than that of P_{ao} along the central vertical line. Figure 2b, c present a comparison of the variances of the capillary pressures (P_{ow} and P_{ao}) between MC and KLME. Considering higher-order terms have been omitted in the KLME derivation, the match is quite reasonable. The variance in P_{ow} rises from 0 at the bottom, to a small salient at the location of the oil leak, and continues to increase with elevation. P_{ao} present a very different behavior, increasing first to a peak at oil leak location, and then decreasing instead of rising. It seems the oil leak affects the behavior of the variance in P_{ao} more than the variance in P_{ow}.

Figure 3 shows the mean (left column) and variance (right column) of fluid pressures along the central vertical line. The mean of each of the three fluid pressures decreases with the elevation, almost linearly for water and air, while oil pressure exhibits some curvature with a salient at the oil leak location. The variance profiles increase with the elevation, and a clear peak occurs at the oil leak location for the variance of oil pressure. The variances are non-linear, with a rapidly increasing variance from the fixed pressure boundary condition at the bottom to the top of the domain. The mean and variance of oil pressure are very sensitive to the oil leak into the domain. The variance in P_a is much smaller than the variance in P_w (7 orders of magnitude larger) and P_o (6 orders of magnitude larger), despite the same order of magnitude for the mean P_a. This is reasonable because air density is nearly 3 orders of magnitude less than liquid densities, and the

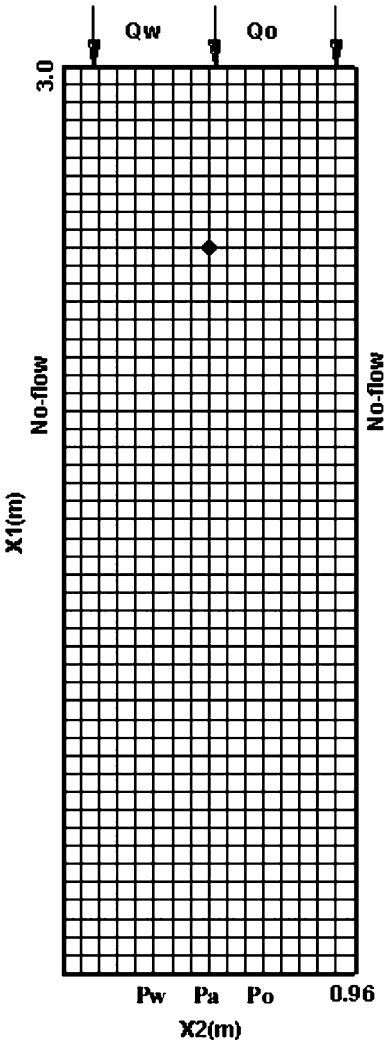

Fig. 1 Model domain and boundary conditions

Table 1 Soil and fluid properties and boundary conditions

Parameter name	Symbol	Units	Case 1	Case 2
Water density	ρ_w	kg/m^3	997.81	997.81
Air density	ρ_a	kg/m^3	1.208	1.208
Oil density	ρ_o	kg/m^3	650	850
Water viscosity	μ_w	Pa s	1.0×10^{-3}	1.0×10^{-3}
Air viscosity	μ_a	Pa s	1.786×10^{-5}	1.786×10^{-5}
Oil viscosity	μ_o	Pa s	6.5×10^{-4}	6.5×10^{-4}
Mean intrinsic permeability	$< k >$	m^2	5.79×10^{-12}	1.52×10^{-8}
Mean oil–water pore size distribution	$< \alpha_{ow} >$	1/Pa	5.53×10^{-4}	1.50×10^{-3}
Mean air–oil pore size distribution	$< \alpha_{ao} >$	1/Pa	1.01×10^{-5}	2.64×10^{-4}
Mean fitting parameter	$< n >$	–	1.36	1.15
Variance permeability	σ^2_k	–	9.52×10^{-24}	8.33×10^{-16}
Variance oil–water pore size distribution	σ^2_{zow}	–	3.11×10^{-9}	1.20×10^{-6}
Variance air–oil pore size distribution	σ^2_{zao}	–	1.04×10^{-12}	5.36×10^{-8}
Variance fitting parameter	σ^2_n	–	1.13×10^{-2}	1.02×10^{-1}
Coefficient of variation (k)	$CV(k)$	–	53.29%	120.81%
Coefficient of variation (α_ ow)	$CV(\alpha\_ow)$	–	10.08%	61.97%
Coefficient of variation (α_ ao)	$CV(\alpha\_ao)$		10.10%	71.40%
Coefficient of variation (n)	$CV(n)$	–	7.86%	27.62%
Correlation length	η_k, η_α, η_n	m	0.3	0.3
Lower boundary water pressure	P_w	Pa	5.00×10^4	9.60×10^4
Lower boundary air pressure	P_a	Pa	5.4×10^4	1.01×10^5
Lower boundary oil pressure	P_o	Pa	5.04×10^4	9.82×10^4
Upper boundary water infiltration	Q_w	cm/year	0.5	3.15
Oil leak rate	D_o	kg/day	100	0.001

Note: Case 1 is simulated and compared with Monte Carlo simulations. Case 2 is served as the base case for sensitivity study of fluid saturation variances

mean air pressure gradient is also about 3 orders of magnitude less (Fig. 3).

Figure 4 presents the mean water, air, and oil saturations on the left column and the corresponding variances on the right column. After 1,000 days, the mean water saturation increases downward from the top of the domain along a smooth curve, with only a very small notch at the oil leak location. This is consistent with full saturation at the water table (X1 = 0). In contrast, the mean air and oil saturations increase upward from the water table, with significant differences in behavior. Air phase saturation (S_a) increases almost linearly upward, although the maximum $S_a < 0.03$, since there is constant water infiltration from the top. The rest of the pore space is occupied by the oil leaked in at the spill location. In each node of the domain, the sum of the three fluid saturations equals 1. The profile of total liquid saturation ($S_{tl} = S_w + S_o = 1 - S_a$) can be derived from the curve of S_a, which decreases upward from the water table (X1 = 0), with a salient at the oil leak location. This behavior can also be determined from the mean air–oil capillary pressure (Fig. 2a) according to van Genuchten relationship between them (Eq. 11). The behavior of the mean saturations and pressures is similar to that of a spill in a homogeneous soil, although not exactly the same since there are some second order non-linearities even in the calculation of the first-order moment.

In addition, the solution of the stochastic partial differential equations (via KLME or MC) allows us to understand the variability in flow behavior due to the soil heterogeneities, through an analysis of the variances. The variances of S_w and S_o increase upward from zero at the water table, where the pressures and saturations are specified as a boundary condition. However, the increase in the variances is not monotonic, since the variances decrease above the oil leak location, with a smooth convexity and sharp salient, respectively. The variance in S_o is more sensitive to the oil leak than the variance in S_w, and exhibits a sharp peak at the oil spill location, indicating significant variability in response near this location, which translates to variability in water saturation in this area as well. In contrast, the variance in S_a is smallest at the oil leak location, since there is very little air in this region.

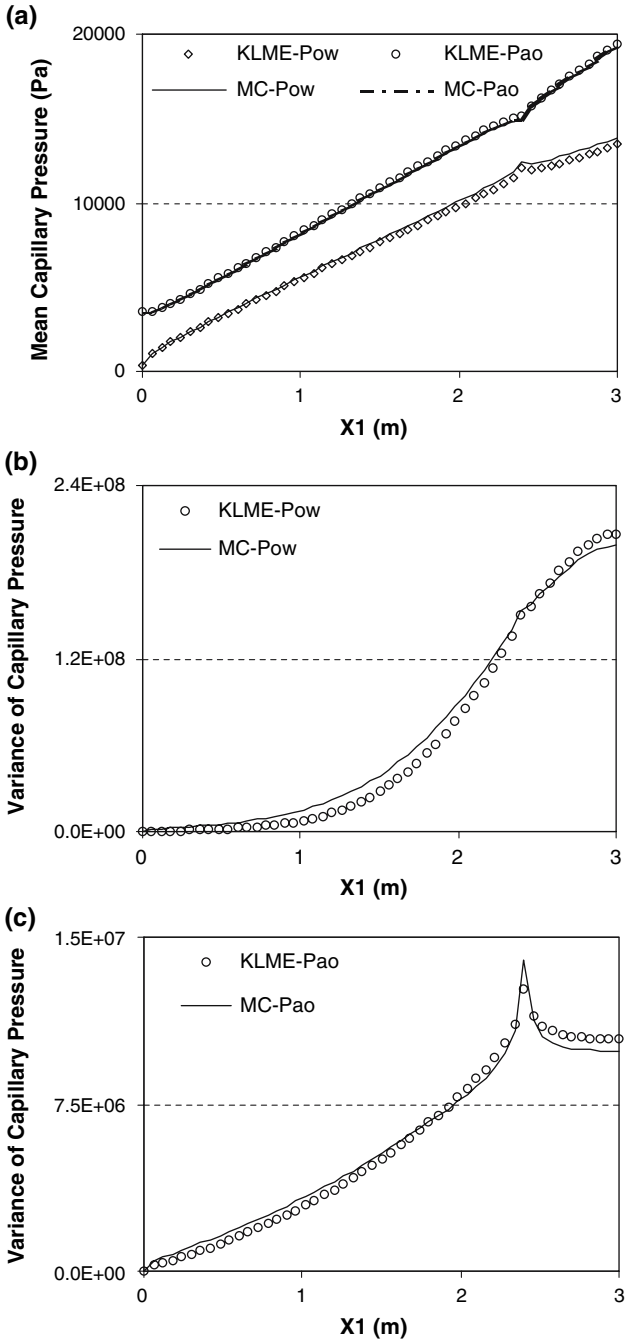

Fig. 2 Comparison between Monte Carlo (*MC*) and KLME stochastic simulations at 1,000 days for central vertical profile of **a** mean capillary pressure, **b** variance of water–oil capillary pressure, and **c** variance of air–oil capillary pressure

In Case 1, Eqs. (30)–(35) are solved for $n = 1, 2, ..., 200$, and the solutions are used to calculate the variances of fluid pressures. Solving coupled, non-linear 0th order KLME partial differential equations cost about ten iterations, and each first order term required about five iterations. The total iterations for KLME in Case 1 are 1,010. As for MC simulations for Case 1, each MC runs took about 20 iterations. The 2,000 MC runs amount to 40,000 iterations, which is 40 times the effort for KLME. The actual time for the KLME simulation in Case 1 was about 1 h, whereas 3 days were spent for the MC simulation in the same computer. This study demonstrates once more that KLME is an efficient approach to investigate the stochastic behavior of multiphase flow, and we will use KLME to conduct sensitivity study of the variances of water, air, and oil saturation to four soil properties variability in Case 2.

4 Case 2: Sensitivity of variances of fluid saturations vs. input variables

The model domain in Case 2 is the same as that in Case 1, while the fluid properties and boundary conditions, as well as the mean and variances of four random input variables, were changed (Table 1). As shown in Fig. 5, the initial oil saturation is less than 0.01 throughout the entire domain, making the modeled area nearly clean unsaturated soil. We reduced the oil leak rate to 0.001 kg/day, but increased water infiltration to 3.15 cm/year, to simulate a slight underground storage tank leak in a wetter climate. As shown in Table 1, the heterogeneity of soil properties was increased substantially in Case 2.

4.1 Transient behavior of variances of fluid pressure

This Case will be used as the base case for sensitivity study of fluid saturation variances to input variability, but first, we would like to discuss the changes of fluid pressure variances with the simulating time. The simulation runs with oil injection for the first 1,000 days, then for another 1,000 days without oil injection. The water infiltration upon the top boundary remains throughout the 2,000 days of simulation time. Figure 6 shows the 2-D contour map of oil pressure variances distributions. With 1,000 days of oil leak at node (2.4 and 0.48 m), the oil pressure variance was distributed radially from oil leak point, and increase upward until the top boundary, due to the water infiltration on the top. After another 1,000 days without oil leak, the local high pressure variances around oil leak location smeared out completely at 2,000 days. However, the oil pressure variances in the lower part of the domain, which is far from the oil leak location, were close to zero and unchanged with the time, which indicates that source/sink term affects the uncertainty of fluid flow significantly. Furthermore, it is seen that the oil pressure variance in Case 1(Fig. 3) is 7 orders of magnitude greater than that in Case 2, despite of much less input variability (Table 1). It is because the oil leak rate in Case 1(100 kg/day) is 5 orders of magnitude larger than that in Case 2

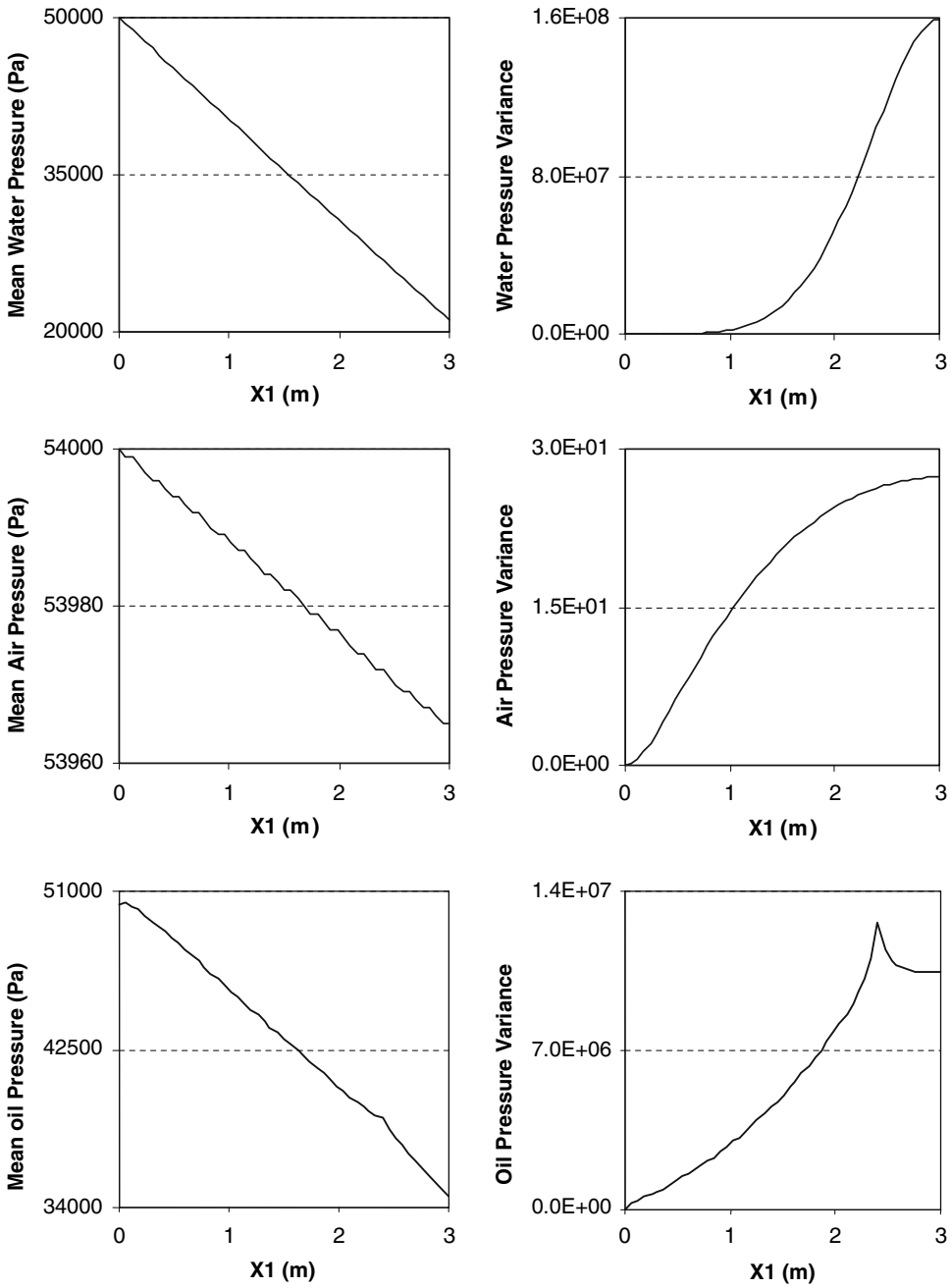

Fig. 3 Mean and variance of water, air and oil pressure at 1,000 days along central vertical line of the domain in Case 1

(0.001 kg/day). This demonstrates that the effect of oil leak upon fluid pressure variances is significant enough to overwhelm the effect of input variances in this study. The change of variances of water and air pressure from 1,000 to 2,000 days is almost negligible compared to that of oil pressure, so we did not show their contour map, from which no apparent change of distribution and magnitude can be seen between the two times. Nevertheless, we do show the changes and the relative changes of the water and air pressure variances, as well as the oil pressure variances, along the central vertical line in Fig. 7. At 1,000 days after stopping oil injection, the oil pressure variances decrease by up to 100%, and the water pressure variances decrease only 0.01%, while air pressure variances increase slightly by 0.002%. This shows the oil injection affects the uncertainty of oil pressure much more than that of water and air pressure.

4.2 The sensitivity of variances of fluid saturation vs. the input variances

To investigate the influence of heterogeneity of soil properties on uncertainty of three-phase flow, we conducted a

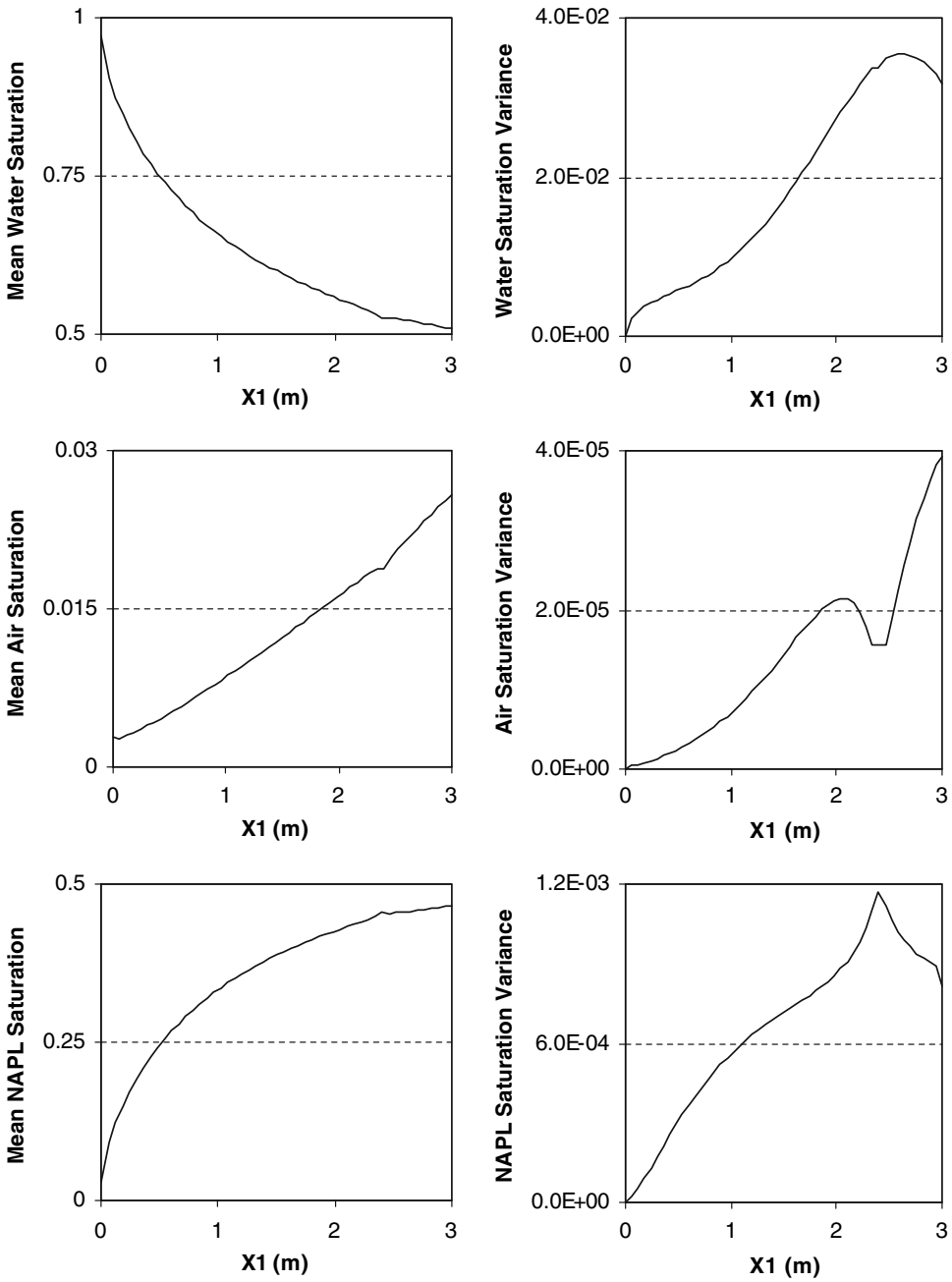

Fig. 4 Mean and variance of water, air and oil saturation at 1,000 days along central vertical line of the domain in Case 1

series of simulations based on Case 2. In each simulation, the variance of one of the four random soil properties, intrinsic permeability Y, oil–water pore size distribution β_{ow}, air–oil pore size distribution β_{ao}, and van Genuchten fitting parameter $\bar{n}$ in Case 2, was increased or decreased by 50%, with the other three unchanged. Thus, a total eight simulations were conducted, and the absolute changes and the relative changes of fluid saturations along the central vertical line of the model domain at 1,000 days with the changed input variability are shown in Figs. 8, 9, 10, and 11.

The effect of intrinsic permeability heterogeneity is presented in Fig. 8. The left column is the results from the simulation with var(Y) increased by 50%, and the right is the one with var(Y) decreased by 50%. The three rows list water, air, and oil saturation variances changes in the two simulations compared to Case 2 simulation. Both changes and relative changes were plotted, corresponding to the left and right y axis, respectively. When var(Y) increased by 50%, the maximum relative changes for variances of water, air, and oil saturation are increased by 0.002%, decrease by 0.0003, and 0.0007%, respectively, as shown in the left column of Fig. 8. Based on these data, we may conclude that the variances of fluid saturation are not so sensitive to intrinsic permeability variability, and the variances of water saturation is relatively

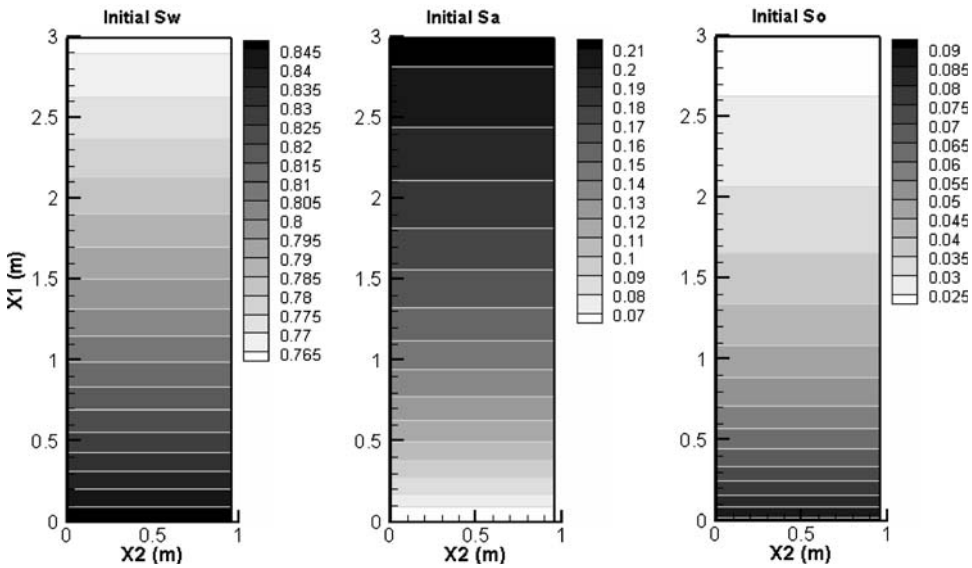

Fig. 5 Initial water, air, and oil saturations in Case 2

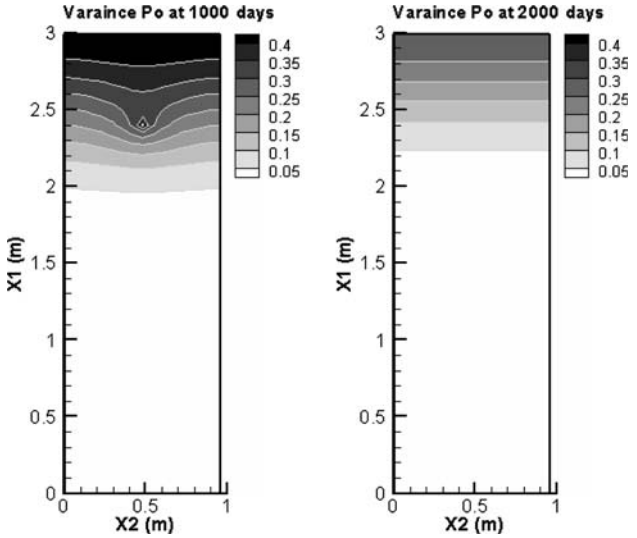

Fig. 6 Contour map of oil pressure variances at 1,000 and 2,000 days in Case 2

more sensitive to variances of Y than air and oil saturation. These results may be related to different phase mobility of water, air and oil, since var(Y) is included in the expression of phase mobility, but not in the van Genuchten model (Eqs. 10, 11), which constructs the relationship between fluid saturation and three random soil properties, excluding intrinsic permeability. When var(Y) decreases 50%, the changes and relative changes of fluid saturation present nearly opposite behavior of the simulation with var(Y) increase by 50%, as shown in the right column of Fig. 8.

Figure 9 presents the sensitivity of variances of fluid saturation to oil–water pore size distribution variability. Apparently, the uncertainty of water saturation is strongly sensitive to variance of β_{ow} (30%), with 4 orders of magnitude larger than those of air (0.0014%) and oil saturation (0.0029%). However, Fig. 10 shows a completely different behavior with regards to the air-oil pore size distribution β_{ao}. The variances of water saturation is insensitive to the variance of β_{ao} (0.008%), while air and oil saturation variability depends substantially on the variance of β_{ao} (35 and 160%). More interesting, the variances of all the three fluid saturations are sensitive to the van Genuchten fitting parameter $\bar{n}$, with maximum relative changes of 43, 38, and 85%, respectively, as shown in Fig. 11. We can resort to the van Genuchten model for a reasonable explanation. From Eq. (10), water saturation is directly dependent on $\alpha_{ow} = \exp(\beta_{ow})$, n, and m, so its variances are sensitive to those of $\beta_{ow}, \bar{n}$. Air saturation $Sa = 1 - St$ depends on $\alpha_{ao} = \exp(\beta_{ao})$, n, and m from Eq. (11), so its variances are related to β_{ao} and $\bar{n}$ strongly. Oil saturation is more related to total liquid saturation St, so the sensitivity of its variances presents the same trend of behavior as air saturation.

In summary, the variances of all three fluid saturations are sensitive to those of $\bar{n}$, but none of them is sensitive to those of Y. In addition, water saturation's variances are also sensitive to those of β_{ow}, and air, oil saturation's variances are sensitive to those of β_{ao}. We summarized the sensitivity study in Table 2.

5 Summary and conclusions

We extended KLME application from transient two-phase flow to transient three-phase flow in this study, and demonstrated its validity and efficiency via numerical implementation by comparison with MC simulations. We then use the verified stochastic three-phase model to

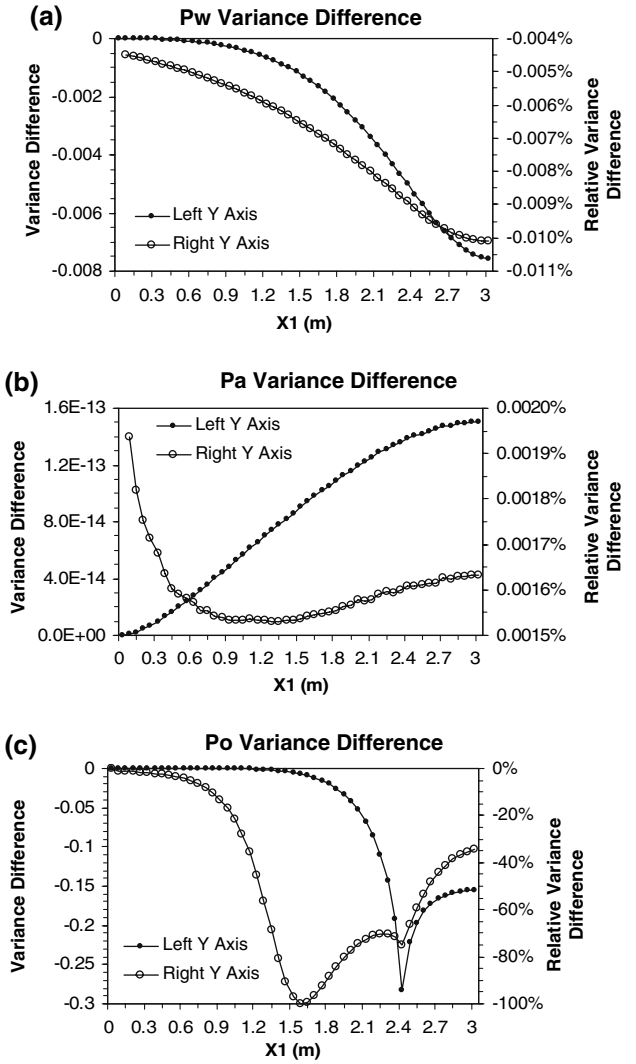

Fig. 7 Changes (*left* *y*-axis) and relative changes (*right* *y*-axis) of variances of **a** water pressure, **b** air pressure, and **c** oil pressure from 1,000 to 2,000 days along central vertical line in Case 2. *Note*: *Y*+ and *Y*− indicates that the variance of *Y* increases and decreases by 50%, respectively. The abscissa of all the figures is central vertical line of the domain (X1); the *left* and *right* ordinate represent the changes and the relative change of the fluid saturation variances in response to the 50% increase or decrease of the intrinsic permeability (*Y*) variances

investigate the sensitivity of variances of fluid saturation to variability of four random soil properties, that is, intrinsic permeability, oil–water pore size distribution, air–oil pore size distribution, and van Genuchten fitting parameter. Based on these discussions, the main findings of this study are summarized as follows:

- The KLME approach is applicable to stochastic analysis of transient three-phase flow with van Genuchten constitutive relationship between fluid saturation and capillary pressure.
- Incorporating the gas phase in the multiphase flow system makes our stochastic model more realistic and applicable than that for water–oil phase flow developed previously (Chen et al. 2005, 2006).
- The comparisons of the KLME and MC simulations validate the applicability of the KLME for three-phase flow, and demonstrate again that the KLME is a more efficient stochastic approach than the traditional MC approach. Thus, it provides a powerful and convenient tool to investigate the stochastic behavior of water–air–oil phase flow in heterogeneous porous media, such as sensitivity analysis.
- The sensitivity analysis for variances of fluid saturation to variability of four different soil properties indicates how and to what extent the different random input variables affect the stochastic behavior of water, air and oil phase flow. To some degree, this analysis serves to better understand the stochastic processes in a multi-phase flow system.

Acknowledgments The authors would like to acknowledge the funding from the Chevron-LANL oil shale project and cooperation between Chevron Energy Technology Company and Los Alamos National Laboratory.

6 Appendix A

The transient part of the governing equation (6) can be expressed as:

$$\phi\frac{\partial S_w}{\partial t}=\phi(1-S_{wr})\frac{\partial \overline{S}_w}{\partial P_{ow}}\cdot\frac{\partial P_{ow}}{\partial t}=C_{ow}\cdot\frac{\partial P_{ow}}{\partial t}, \tag{40}$$

$$\phi\frac{\partial S_a}{\partial t}=-\phi(1-S_{wr})\frac{\partial \overline{S}_t}{\partial P_{ao}}\cdot\frac{\partial P_{ao}}{\partial t}=C_{ao}\cdot\frac{\partial P_{ao}}{\partial t}, \tag{41}$$

$$\phi\frac{\partial S_o}{\partial t}=\phi\frac{\partial(1-S_w-S_a)}{\partial t}=-\left(C_{ow}\cdot\frac{\partial P_{ow}}{\partial t}+C_{ao}\cdot\frac{\partial P_{ao}}{\partial t}\right), \tag{42}$$

where

$$\begin{aligned}C_{ow}(\mathbf{x},t)&=\phi(1-S_{wr})\frac{\partial \overline{S}_w}{\partial P_{ow}}\\&=-\phi(1-S_{wr})\alpha_{ow}(n-1)\overline{S}_w^{1/m}\left[1-\overline{S}_w^{1/m}\right]^m,\end{aligned} \tag{43}$$

$$\begin{aligned}C_{ao}(\mathbf{x},t)&=-\phi(1-S_{wr})\frac{\partial \overline{S}_t}{\partial P_{ao}}\\&=\phi(1-S_{wr})\alpha_{ao}(n-1)\overline{S}_t^{1/m}\left[1-\overline{S}_t^{1/m}\right]^m.\end{aligned} \tag{44}$$

The log transformed water, air and oil phase mobility $Z_p = \ln \lambda_p$ can be derived as follows:

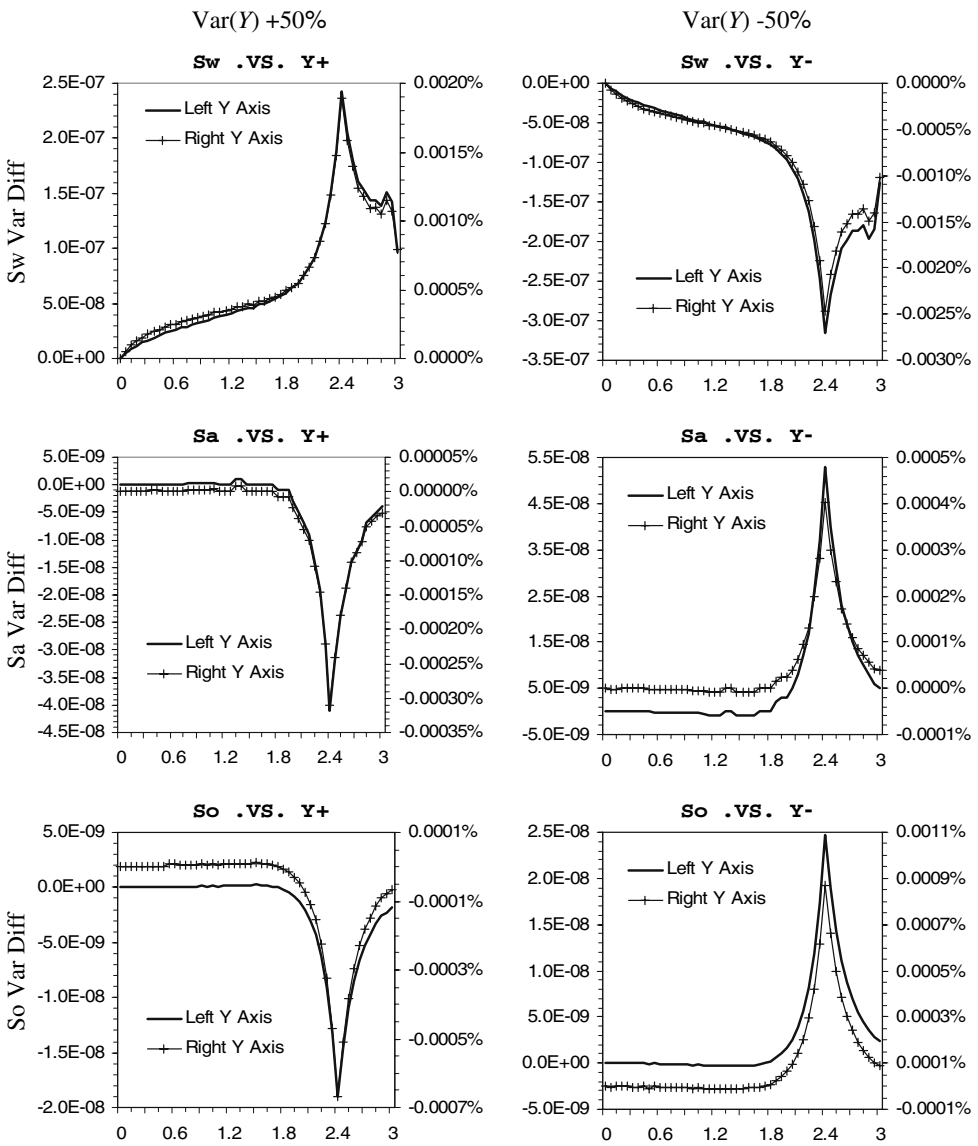

Fig. 8 The change of the variances of water, air, and oil saturation with the 50% increase and decrease of the variances of the soil intrinsic permeability. *Note*: β_{ow}+ and β_{ow}− indicates that the variance of β_{ow} increase and decrease by 50%, respectively. The abscissa of all the figures is central vertical line of the domain (X1); the *left* and *right* ordinate represent the changes and the relative change of fluid saturation variances in response to the 50% increase or decrease of the oil–water pore size distribution (β_{ow}) variances

$$Z_w = \ln \lambda_w = Y - \ln \mu_w + \frac{1}{2}\ln \overline{S}_w + 2\ln\left[1 - \left(1 - \overline{S}_w^{1/m}\right)^m\right], \quad (45)$$

$$Z_a = \ln \lambda_a = Y - \ln \mu_a + \frac{1}{2}\ln\left(1 - \overline{S}_t\right) + 2m \ln\left(1 - \overline{S}_t^{1/m}\right), \quad (46)$$

$$Z_o = \ln \lambda_o = Y - \ln \mu_o + \frac{1}{2}\ln\left(\overline{S}_t - \overline{S}_w\right) + 2\ln\left[\left(1 - \overline{S}_w^{1/m}\right)^m - \left(1 - \overline{S}_t^{1/m}\right)^m\right]. \quad (47)$$

On the basis of (45)–(47) and (43), (44), we can obtain

$$Z_w^{(0)}(\mathbf{x},t) = Y - \ln \mu_w + \frac{1}{2}\ln \overline{S}_w^{(0)} + 2\ln\left[1 - \left(1 - \overline{S}_w^{(0)1/\langle m\rangle}\right)^{\langle m\rangle}\right], \quad (48)$$

$$Z_a^{(0)}(\mathbf{x},t) = Y - \ln \mu_a + \frac{1}{2}\ln\left(1 - \overline{S}_t^{(0)}\right) + 2\langle m\rangle \ln\left(1 - \overline{S}_t^{(0)1/\langle m\rangle}\right), \quad (49)$$

$$Z_o^{(0)}(\mathbf{x},t) = Y - \ln \mu_o + \frac{1}{2}\ln\left(\overline{S}_t^{(0)} - \overline{S}_w^{(0)}\right) + 2\ln\left[\left(1 - \overline{S}_w^{(0)1/\langle m\rangle}\right)^{\langle m\rangle} - \left(1 - \overline{S}_t^{(0)1/\langle m\rangle}\right)^{\langle m\rangle}\right], \quad (50)$$

$$C_{ow}^{(0)}(\mathbf{x},t) = -\phi(1 - S_{wr})e^{\langle\beta_{ow}\rangle}e^{\langle\bar{n}\rangle}\overline{S}_w^{(0)1/\langle m\rangle}\left[1 - \overline{S}_w^{(0)1/\langle m\rangle}\right]^{\langle m\rangle}, \quad (51)$$

$$C_{ao}^{(0)}(\mathbf{x},t) = \phi(1 - S_{wr})e^{\langle\beta_{ao}\rangle}e^{\langle\bar{n}\rangle}\overline{S}_t^{(0)1/\langle m\rangle}\left[1 - \overline{S}_t^{(0)1/\langle m\rangle}\right]^{\langle m\rangle}, \quad (52)$$

and

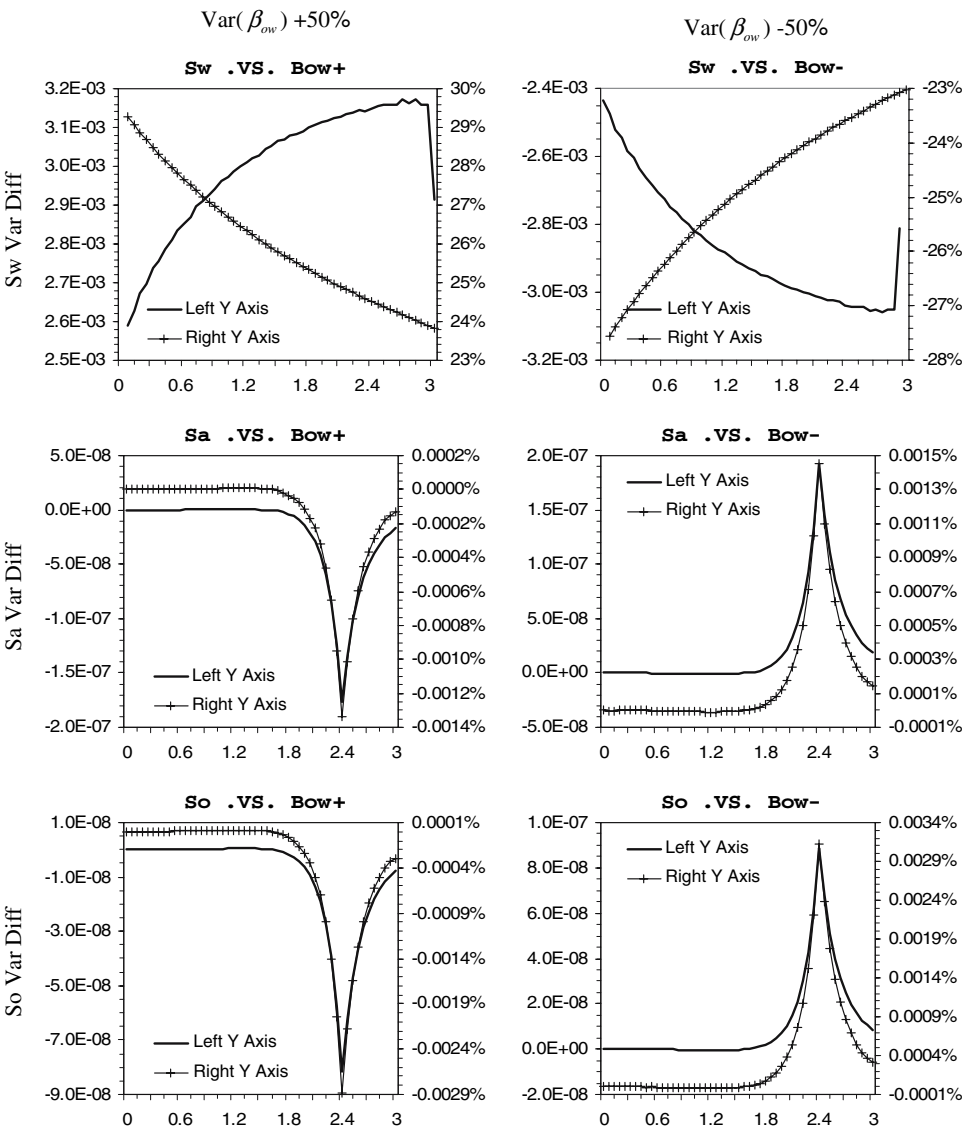

Fig. 9 The change of the variances of water, air, and oil saturation with the 50% increase and decrease of the variances of the oil–water pore size distribution. *Note*: $\beta_{ao}+$ and $\beta_{ao}-$ indicates that the variance of β_{ao} increase and decrease by 50%, respectively. The abscissa of all the figures is central vertical line of the domain (X1); the *left* and *right* ordinate represent the changes and the relative change of the fluid saturation variances in response to the 50% increase or decrease of the air–oil pore size distribution (β_{ao}) variances

$$Z_w^{(1)}(\mathbf{x},t) = Y' + u_{w,100}P_{ow}^{(1)} + u_{w,010}\beta'_{ow} + u_{w,001}\bar{n}', \tag{53}$$

$$Z_a^{(1)}(\mathbf{x},t) = Y' + u_{a,100}P_{ao}^{(1)} + u_{a,010}\beta'_{ao} + u_{a,001}\bar{n}', \tag{54}$$

$$Z_o^{(1)}(\mathbf{x},t) = Y' + u_{o,10000}P_{ow}^{(1)} + u_{o,01000}P_{ao}^{(1)} + u_{o,00100}\beta'_{ow} + u_{o,00010}\beta'_{ao} + u_{o,00001}\bar{n}', \tag{55}$$

$$C_{ow}^{(1)}(\mathbf{x},t) = v_{w,100}P_{ow}^{(1)} + v_{w,010}\beta'_{ow} + v_{w,001}\bar{n}', \tag{56}$$

$$C_{ao}^{(1)}(\mathbf{x},t) = v_{a,100}P_{ao}^{(1)} + v_{a,010}\beta'_{ao} + v_{a,001}\bar{n}', \tag{57}$$

where,

$$u_{w,ijk}(\mathbf{x},t) = \frac{\partial^{i+j+k}Z_w(\mathbf{x},t)}{\partial P_{ow}^i \partial \beta_{ow}^j \partial \bar{n}^k}, \tag{58}$$

$$u_{a,ijk}(\mathbf{x},t) = \frac{\partial^{i+j+k}Z_a(\mathbf{x},t)}{\partial P_{ao}^i \partial \beta_{ao}^j \partial \bar{n}^k}, \tag{59}$$

$$u_{o,ijklm}(\mathbf{x},t) = \frac{\partial^{i+j+k+l+m}Z_o(\mathbf{x},t)}{\partial P_{ow}^i \partial P_{ao}^j \partial \beta_{ow}^k \partial \beta_{ao}^l \partial \bar{n}^m}, \tag{60}$$

$$v_{w,ijk}(\mathbf{x},t) = \frac{\partial^{i+j+k}C_{ow}(\mathbf{x},t)}{\partial P_{ow}^i \partial \beta_{ow}^j \partial \bar{n}^k}, \tag{61}$$

$$v_{a,ijk}(\mathbf{x},t) = \frac{\partial^{i+j+k}C_{ao}(\mathbf{x},t)}{\partial P_{ao}^i \partial \beta_{ao}^j \partial \bar{n}^k}. \tag{62}$$

Equations (58)–(62) are evaluated at $P_{ow}^{(0)}(\mathbf{x},t), P_{ao}^{(0)}(\mathbf{x},t)$, $\langle\beta_{ow}(\mathbf{x})\rangle, \langle\beta_{ao}(\mathbf{x})\rangle$, and $\langle\bar{n}(\mathbf{x})\rangle$. Their explicit expressions are given in Appendix B. The KL expansion of the

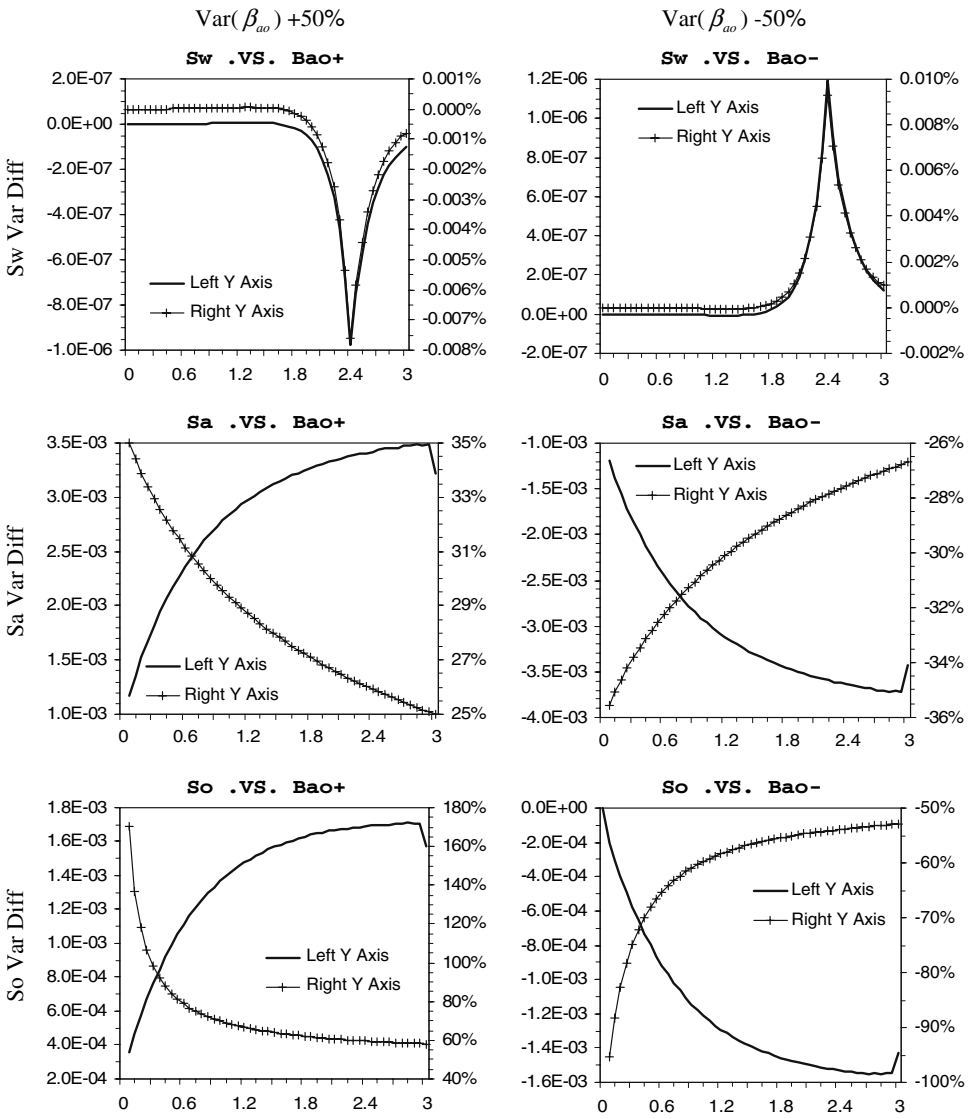

Fig. 10 The change of the variances of water, air, and oil saturation with the 50% increase and decrease of the variances of the air–oil pore size distribution. *Note*: $\bar{n}+$ and $\bar{n}-$ indicates that the variance of $\bar{n}$ increase and decrease by 50%, respectively. The abscissa of all the figures is central vertical line of the domain (X1); the *left* and *right* ordinate represent the changes and the relative change of the fluid saturation variances in response to the 50% increase or decrease of the van Genuchten fitting parameter ($\bar{n}$) variances

fluctuation part of log-transformed soil permeability can be expressed as (Chen et al. 2005):

$$Y'(\mathbf{x},\theta) = \sum_{n=1}^{\infty} \xi_n(\theta)\sqrt{\lambda_n} f_n(\mathbf{x}) = \sum_{n=1}^{\infty} \xi_n(\theta)\bar{f}_n(\mathbf{x}). \tag{63}$$

In the above equation, λ_n, $f_n(\mathbf{x})$ are eigenvalue and the corresponding eigenfunction of covariance $C_Y(\mathbf{x},\mathbf{y})$, respectively, and $\sqrt{\lambda_n}, f_n(\mathbf{x})$ are combined into $\bar{f}_n(\mathbf{x})$, since $\sqrt{\lambda_n}$ and $f_n(\mathbf{x})$ are always coupled. $\bar{f}_n(\mathbf{x})$ will be written as $f_n(\mathbf{x})$ in the following formulation for simplicity. Similarly, the KL expansion of the log pore-size distribution parameters $\beta_{ow}(\mathbf{x})$, $\beta_{ao}(\mathbf{x})$, and fitting parameter $\bar{n}(\mathbf{x})$ are:

$$\beta'_{ow}(\mathbf{x},\theta) = \sum_{n=1}^{\infty} \xi_n(\theta)\phi_n(\mathbf{x}), \tag{64}$$

$$\beta'_{ao}(\mathbf{x},\theta) = \sum_{n=1}^{\infty} \xi_n(\theta)\varphi_n(\mathbf{x}), \tag{65}$$

$$\bar{n}'(\mathbf{x},\theta) = \sum_{n=1}^{\infty} \xi_n(\theta)\psi_n(\mathbf{x}), \tag{66}$$

where, $\phi_n(\mathbf{x})$, $\varphi_n(\mathbf{x})$, and $\psi_n(\mathbf{x})$ are respectively the product of the square root of an eigenvalue and its corresponding eigenfunction of covariance $C_{\beta ow}(\mathbf{x},\mathbf{y})$, $C_{\beta ao}(\mathbf{x},\mathbf{y})$ and $C_{\bar{n}}(\mathbf{x},\mathbf{y})$.

The terms $P_p^{(1)}(\mathbf{x},t), Z_p^{(1)}(\mathbf{x},t), C_{ow}^{(1)}(\mathbf{x},t)$, and $C^{(1)}{}_{ao}(\mathbf{x},t)$ in equations (24) to (29) in the text can be expressed in terms of a set of orthogonal Gaussian random variables $\{\xi_n\}$ and deterministic coefficients $P_{p,n}^{(1)}(\mathbf{x},t), Z_{p,n}^{(1)}(\mathbf{x},t), C_{ow,n}^{(1)}(\mathbf{x},t)$, and $C^{(1)}{}_{ao,n}(\mathbf{x},t)$:

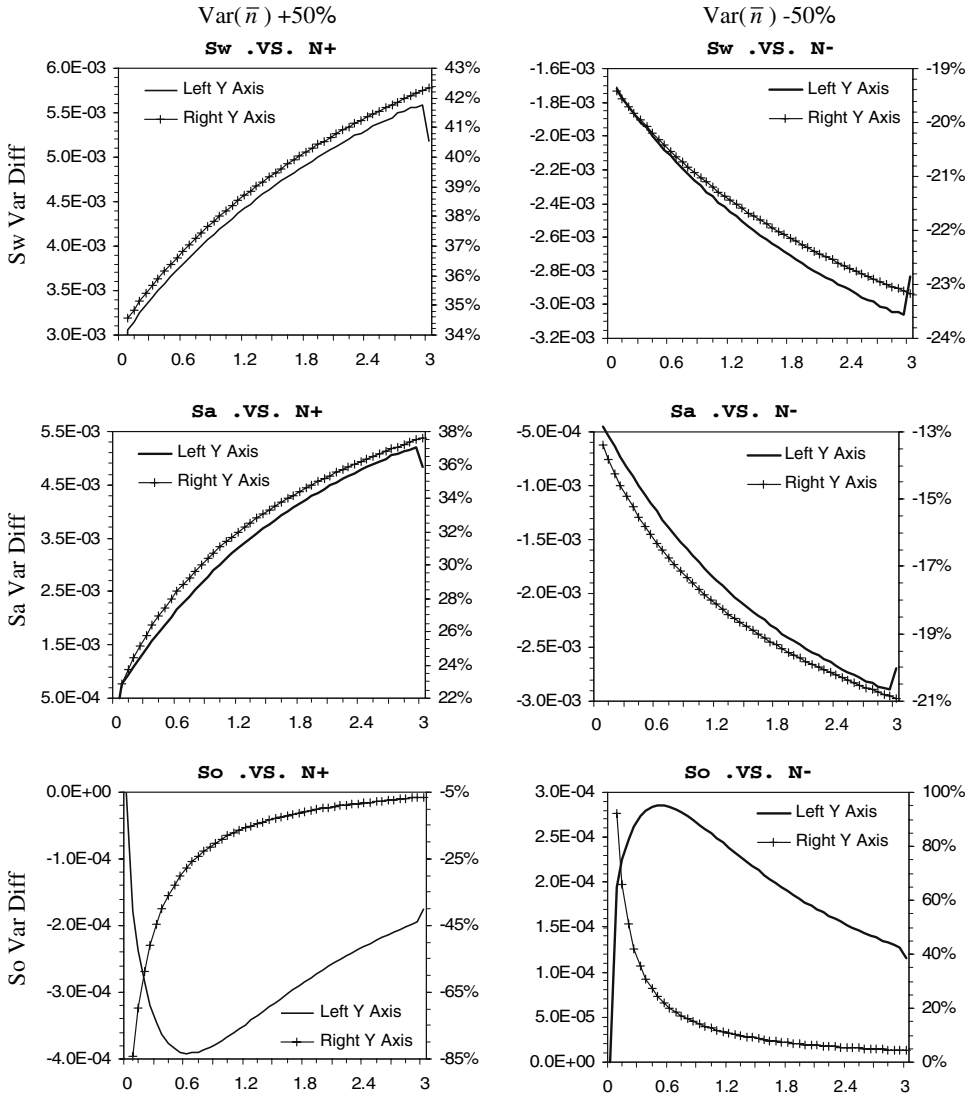

Fig. 11 The change of the variances of water, air, and oil saturation with the 50% increase and decrease of the variances of the van Genuchten fitting parameter

Table 2 Sensitivity of variances of fluid saturation to input variability

	Y	β_{ow}	β_{ao}	$\bar{n}$
Sw	−	+	−	+
Sa	−	−	+	+
So	−	−	+	+

Note: + indicates sensitive, − indicates insensitive

$$P_p^{(1)}(\mathbf{x},t) = \sum_{n=1}^{\infty} \xi_n P_{p,n}^{(1)}(\mathbf{x},t), \tag{67}$$

$$Z_p^{(1)}(\mathbf{x},t) = \sum_{n=1}^{\infty} \xi_n Z_{p,n}^{(1)}(\mathbf{x},t), \tag{68}$$

$$C_{ow}^{(1)}(\mathbf{x},t) = \sum_{n=1}^{\infty} \xi_n C_{ow,n}^{(1)}(\mathbf{x},t), \tag{69}$$

$$C_{ao}^{(1)}(\mathbf{x},t) = \sum_{n=1}^{\infty} \xi_n C_{ao,n}^{(1)}(\mathbf{x},t) \tag{70}$$

based on (53) to (57) and (63) to (66),

$$Z_{w,n}^{(1)}(\mathbf{x},t) = f_n + u_{w,100} P_{ow,n}^{(1)} + u_{w,010}\phi_n + u_{w,001}\psi_n, \tag{71}$$

$$Z_{a,n}^{(1)}(\mathbf{x},t) = f_n + u_{a,100} P_{ao,n}^{(1)} + u_{a,010}\varphi_n + u_{a,001}\psi_n, \tag{72}$$

$$\begin{aligned} Z_{o,n}^{(1)}(\mathbf{x},t) = f_n &+ u_{o,10000} P_{ow,n}^{(1)} + u_{o,01000} P_{ao,n}^{(1)} + u_{o,00100}\phi_n \\ &+ u_{o,00010}\varphi_n + u_{o,00001}\psi_n, \end{aligned} \tag{73}$$

$$C_{ow,n}^{(1)}(\mathbf{x},t) = v_{w,100} P_{ow,n}^{(1)} + v_{w,010}\phi_n + v_{w,001}\psi_n, \tag{74}$$

$$C^{(1)}_{ao,n}(\mathbf{x},t) = v_{a,100}P^{(1)}_{ao,n} + v_{a,010}\varphi_n + v_{a,001}\psi_n. \tag{75}$$

7 Appendix B

As shown in the text, $Z_p(\mathbf{x},t)$, $C_{ow}(\mathbf{x},t)$, $C_{ao}(\mathbf{x},t)$ are function of capillary pressure, pore size distribution and van Genuchten fitting parameters, all of which are stochastic.

$$u_{w,100} = \frac{\partial Z_w}{\partial P_{ow}} = \frac{\partial Z_w}{\partial \bar{S}_w}\cdot\frac{\partial \bar{S}_w}{\partial P_{ow}}, \quad u_{a,100} = \frac{\partial Z_a}{\partial P_{ao}} = \frac{\partial Z_a}{\partial \bar{S}_t}\cdot\frac{\partial \bar{S}_t}{\partial P_{ao}}, \tag{76}$$

$$u_{w,010} = \frac{\partial Z_w}{\partial \beta_{ow}} = \frac{\partial Z_w}{\partial \bar{S}_w}\cdot\frac{\partial \bar{S}_w}{\partial \beta_{ow}}, \quad u_{a,010} = \frac{\partial Z_a}{\partial \beta_{ao}} = \frac{\partial Z_a}{\partial \bar{S}_t}\cdot\frac{\partial \bar{S}_t}{\partial \beta_{ao}}, \tag{77}$$

$$u_{w,001} = \frac{\partial Z_w}{\partial \bar{n}} = \frac{\partial Z_w}{\partial n}\cdot\frac{\partial n}{\partial \bar{n}} = e^{\bar{n}}\frac{\partial Z_w}{\partial n}, \tag{78}$$

where,

$$\frac{\partial Z_w}{\partial n} = \frac{\partial Z_w}{\partial \bar{S}_w}\cdot\frac{\partial \bar{S}_w}{\partial n} - \left(\frac{2}{n^2}\right)\frac{\left(1-\bar{S}_w^{1/m}\right)^m}{1-\left(1-\bar{S}_w^{1/m}\right)^m} \times\left[\ln\left(1-\bar{S}_w^{1/m}\right) + \frac{\bar{S}_w^{1/m}}{1-\bar{S}_w^{1/m}}\left(\frac{\ln \bar{S}_w}{m}\right)\right], \tag{79}$$

$$u_{a,001} = \frac{\partial Z_a}{\partial \bar{n}} = \frac{\partial Z_a}{\partial n}\cdot\frac{\partial n}{\partial \bar{n}} = e^{\bar{n}}\frac{\partial Z_a}{\partial n}, \tag{80}$$

where,

$$\frac{\partial Z_a}{\partial n} = \frac{\partial Z_a}{\partial \bar{S}_t}\cdot\frac{\partial \bar{S}_t}{\partial n} + \left(\frac{2}{n^2}\right)\left[\ln\left(1-\bar{S}_t^{1/m}\right) + \frac{\bar{S}_t^{1/m}}{1-\bar{S}_t^{1/m}}\left(\frac{\ln \bar{S}_t}{m}\right)\right]. \tag{81}$$

Similarly,

$$v_{w,100} = \frac{\partial C_{ow}}{\partial P_{ow}} = \frac{\partial C_{ow}}{\partial \bar{S}_w}\cdot\frac{\partial \bar{S}_w}{\partial P_{ow}}, \tag{82}$$

$$v_{w,010} = \frac{\partial C_{ow}}{\partial \beta_{ow}} = \frac{\partial C_{ow}}{\partial \bar{S}_w}\cdot\frac{\partial \bar{S}_w}{\partial \beta_{ow}} + C_{ow}(\mathbf{x},t), \tag{83}$$

$$v_{w,001} = \frac{\partial C_{ow}}{\partial \bar{n}} = \frac{\partial C_{ow}}{\partial n}\cdot\frac{\partial n}{\partial \bar{n}} = e^{\bar{n}}\frac{\partial C_{ow}}{\partial n}, \tag{84}$$

where,

$$\frac{\partial C_{ow}}{\partial n} = \frac{\partial C_{ow}}{\partial \bar{S}_w}\frac{\partial \bar{S}_w}{\partial n} + \frac{C_{ow}(\mathbf{x},t)}{(n-1)^2} \times\left[n-1+m^2\ln\left(1-\bar{S}_w^{1/m}\right) + \frac{(m+1)\bar{S}_w^{1/m}-1}{1-\bar{S}_w^{1/m}}\ln \bar{S}_w\right], \tag{85}$$

and

$$v_{a,100} = \frac{\partial C_{ao}}{\partial P_{ao}} = \frac{\partial C_{ao}}{\partial \bar{S}_t}\cdot\frac{\partial \bar{S}_t}{\partial P_{ao}}, \tag{86}$$

$$v_{a,010} = \frac{\partial C_{ao}}{\partial \beta_{ao}} = \frac{\partial C_{ao}}{\partial \bar{S}_t}\cdot\frac{\partial \bar{S}_t}{\partial \beta_{ao}} + C_{ao}(\mathbf{x},t), \tag{87}$$

$$v_{a,001} = \frac{\partial C_{ao}}{\partial \bar{n}} = \frac{\partial C_{ao}}{\partial n}\cdot\frac{\partial n}{\partial \bar{n}} = e^{\bar{n}}\frac{\partial C_{ao}}{\partial n}, \tag{88}$$

where,

$$\frac{\partial C_{ao}}{\partial n} = \frac{\partial C_{ao}}{\partial \bar{S}_t}\frac{\partial \bar{S}_t}{\partial n} + \frac{C_{ao}(\mathbf{x},t)}{(n-1)^2} \times\left[n-1+m^2\ln\left(1-\bar{S}_t^{1/m}\right) + \frac{(m+1)\bar{S}_t^{1/m}-1}{1-\bar{S}_t^{1/m}}\ln \bar{S}_t\right]. \tag{89}$$

The above equations are evaluated at $P^{(0)}_{ow}, P^{(0)}_{ao}$, $\langle\beta_{ow}\rangle, \langle\beta_{ao}\rangle, \langle\bar{n}\rangle$ and $\bar{S}^{(0)}_w, \bar{S}^{(0)}_t$.

$$\overline{S}^{(0)}_w(\mathbf{x},t) = \left[1+\left(e^{\langle\beta ow\rangle}P^{(0)}_{ow}\right)^{\langle n\rangle}\right]^{-\langle m\rangle}, \tag{90}$$

$$\overline{S}^{(0)}_t(\mathbf{x},t) = \left[1+\left(e^{\langle\beta ao\rangle}P^{(0)}_{ao}\right)^{\langle n\rangle}\right]^{-\langle m\rangle}, \tag{91}$$

where, $\langle n\rangle = e^{\langle\bar{n}\rangle}+1, \langle m\rangle = 1-1/\langle n\rangle$.

Among the equations above,

$$\frac{\partial Z_w}{\partial \bar{S}_w} = \frac{1}{2\bar{S}_w} + \frac{2\left(\bar{S}_w^{-1/m}-1\right)^{m-1}}{1-\left(1-\bar{S}_w^{1/m}\right)^m}, \tag{92}$$

$$\frac{\partial Z_a}{\partial \bar{S}_t} = \frac{-1}{2(1-\bar{S}_t)} - \frac{2\bar{S}_t^{-1}}{\bar{S}_t^{-1/m}-1}, \tag{93}$$

$$\frac{\partial \bar{S}_w}{\partial P_{ow}} = -\frac{n-1}{P_{ow}}\bar{S}_w\left(1-\bar{S}_w^{1/m}\right), \tag{94}$$

$$\frac{\partial \bar{S}_w}{\partial \beta_{ow}} = -(n-1)\bar{S}_w\left(1-\bar{S}_w^{1/m}\right), \tag{95}$$

$$\frac{\partial \bar{S}_t}{\partial P_{ao}} = -\frac{n-1}{P_{ao}}\bar{S}_t\left(1-\bar{S}_t^{1/m}\right), \tag{96}$$

$$\frac{\partial \bar{S}_t}{\partial \beta_{ao}} = -(n-1)\bar{S}_t\left(1-\bar{S}_t^{1/m}\right), \tag{97}$$

$$\frac{\partial C_{ow}}{\partial \bar{S}_w} = -\phi(1-S_{wr})\cdot e^{\beta ow} \cdot\bar{S}_w^{1/m-1}\left(1-\bar{S}_w^{1/m}\right)^{m-1}\left[n-(2n-1)\bar{S}_w^{1/m}\right], \tag{98}$$

$$\frac{\partial C_{ao}}{\partial \bar{S}_t} = \phi(1-S_{wr})\cdot e^{\beta ao} \cdot\bar{S}_t^{1/m-1}\left(1-\bar{S}_t^{1/m}\right)^{m-1}\left[n-(2n-1)\bar{S}_t^{1/m}\right], \tag{99}$$

$$\frac{\partial \bar{S}_w}{\partial n} = \frac{\bar{S}_w(\ln \bar{S}_w)}{n(n-1)} - \frac{m}{n}\bar{S}_w\left(1-\bar{S}_w^{1/m}\right)\ln\left[\bar{S}_w^{-1/m}-1\right], \tag{100}$$

$$\frac{\partial \bar{S}_t}{\partial n} = \frac{\bar{S}_t(\ln \bar{S}_t)}{n(n-1)} - \frac{m}{n}\bar{S}_t\left(1-\bar{S}_t^{1/m}\right)\ln\left[\bar{S}_t^{-1/m}-1\right]. \tag{101}$$

Consider NAPL phase mobility,

$$u_{o,10000} = \frac{\partial Z_o}{\partial P_{ow}} = \frac{\partial Z_o}{\partial \bar{S}_w}\cdot\frac{\partial \bar{S}_w}{\partial P_{ow}}, \tag{102}$$

$$u_{o,01000} = \frac{\partial Z_o}{\partial P_{ao}} = \frac{\partial Z_o}{\partial \bar{S}_t}\cdot\frac{\partial \bar{S}_t}{\partial P_{ao}}, \tag{103}$$

$$u_{o,00100} = \frac{\partial Z_o}{\partial \beta_{ow}} = \frac{\partial Z_o}{\partial \bar{S}_w}\cdot\frac{\partial \bar{S}_w}{\partial \beta_{ow}}, \tag{104}$$

$$u_{o,00010} = \frac{\partial Z_o}{\partial \beta_{ao}} = \frac{\partial Z_o}{\partial \bar{S}_t}\cdot\frac{\partial \bar{S}_t}{\partial \beta_{ao}}, \tag{105}$$

$$u_{o,00001} = \frac{\partial Z_o}{\partial \bar{n}} = \frac{\partial Z_o}{\partial n}\cdot\frac{\partial n}{\partial \bar{n}} = e^{\bar{n}}\frac{\partial Z_o}{\partial n}, \tag{106}$$

where,

$$\frac{\partial Z_o}{\partial \bar{S}_w} = \frac{1}{2(\bar{S}_t-\bar{S}_w)} - \frac{2\left(\bar{S}_w^{-1/m}-1\right)^{m-1}}{\left(1-\bar{S}_w^{1/m}\right)^m - \left(1-\bar{S}_t^{1/m}\right)^m}, \tag{107}$$

$$\frac{\partial Z_o}{\partial \bar{S}_t} = \frac{1}{2(\bar{S}_t-\bar{S}_w)} + \frac{2\left(\bar{S}_t^{-1/m}-1\right)^{m-1}}{\left(1-\bar{S}_w^{1/m}\right)^m - \left(1-\bar{S}_t^{1/m}\right)^m}, \tag{108}$$

$$\begin{aligned}\frac{\partial Z_o}{\partial n} = {} & \frac{\partial Z_o}{\partial \bar{S}_w}\cdot\frac{\partial \bar{S}_w}{\partial n} + \frac{\partial Z_o}{\partial \bar{S}_t}\cdot\frac{\partial \bar{S}_t}{\partial n} \\ & - \left(\frac{2}{n^2}\right)\frac{1}{\left(1-\bar{S}_w^{1/m}\right)^m - \left(1-\bar{S}_t^{1/m}\right)^m} \\ & \times\left\{\left(1-\bar{S}_w^{1/m}\right)^m\left[\ln\left(1-\bar{S}_w^{1/m}\right) + \frac{\bar{S}_w^{1/m}}{1-\bar{S}_w^{1/m}}\left(\frac{\ln \bar{S}_w}{m}\right)\right]\right. \\ & \left. - \left(1-\bar{S}_t^{1/m}\right)^m\left[\ln\left(1-\bar{S}_t^{1/m}\right) + \frac{\bar{S}_t^{1/m}}{1-\bar{S}_t^{1/m}}\left(\frac{\ln \bar{S}_t}{m}\right)\right]\right\}.\end{aligned} \tag{109}$$

References

Abdin A, Kaluarachchi JJ (1997a) Stochastic analysis of three-phase flow in heterogeneous porous media: I. Spectral/perturbation approach. Water Resour Res 33(7):1549–1558

Abdin A, Kaluarachchi JJ (1997b) Stochastic analysis of three-phase flow in heterogeneous porous media: II. Numerical simulations. Water Resour Res 33(7):1559–1566

Abdin A, Kaluarachchi JJ, Chang C, Kemblowski MW (1995) Stochastic analysis of multiphase flow in porous media: II. Comparison with Monte Carlo simulations. Transp Porous Media 19(3):261–280

Abdin A, Kaluarachchi JJ, Chang C, Kemblowski MW (1996) Stochastic analysis of multiphase flow in porous media: II. Comparison with Monte Carlo simulations. Stochastic Hydrol Hydraul 10:231–251

Chang C, Kemblowski MW, Kaluarachchi JJ, Abdin A (1995a) Stochastic analysis of multiphase flow in porous media, I, Spectral/perturbation analysis. Transp Porous Media 19(3):233–259

Chang C, Kemblowski MW, Kaluarachchi JJ, Abdin A (1995b) Stochastic analysis of multiphase flow in porous media, I, Spectral/perturbation analysis. Stochastic Hydrol Hydraul 9:39–267

Chen M, Zhang D, Keller AA, Lu Z (2005) A stochastic analysis of steady state two-phase flow in heterogeneous media. Water Resour Res 41(1):w01006. doi:10.1029/2004WR003412

Chen M, Zhang D, Keller AA, Lu Z, Zyvoloski GA (2006) A Stochastic analysis of transient two-phase flow in heterogeneous porous media. Water Resour Res 42:W03425. doi:10.1029/2005WR004257

Dagan G (1989) Flow and transport in porous formations. Springer, New York

Gelhar W (1993) Stochastic subsurface hydrology. Prentice-Hall, Englewood Cliffs

Ghanem G, Dham S (1998) Stochastic finite element analysis for multiphase flow in heterogeneous media. Transport Porous Media 32:239–262

Trangenstein J, Bell J (1989) Mathematical structure of the black-oil model for petroleum reservoir simulation. SIAM J Appl Math 49(3):749–783

Yang J, Zhang D, Lu Z (2004) Stochastic analysis of saturated-unsaturated flow in heterogeneous media by combining Karhunen–Loeve expansion and perturbation method. J Hydrol 294:18–38

Zhang D (2002) Stochastic methods for flow in porous media: coping with uncertainties. Academic, San Diego, ISBN 012–7796215, p 350

Zhang D, Lu Z (2004) Evaluation of higher-order moments for saturated flow in randomly heterogeneous media via Karhunen–Loeve decomposition. J Comput Phys 194:773–794